



HAL
open science

Glass formation and devitrification behavior of alkali (Li, Na) aluminosilicate melts containing TiO₂

Alessio Zandonà, Sandra Ory, Cécile Genevois, Emmanuel Véron, Aurélien Canizarès, Michael J Pitcher, Mathieu Allix

► To cite this version:

Alessio Zandonà, Sandra Ory, Cécile Genevois, Emmanuel Véron, Aurélien Canizarès, et al.. Glass formation and devitrification behavior of alkali (Li, Na) aluminosilicate melts containing TiO₂. *Journal of Non-Crystalline Solids*, 2022, 582, pp.121448. 10.1016/j.jnoncrysol.2022.121448 . hal-03562671

HAL Id: hal-03562671

<https://hal.science/hal-03562671>

Submitted on 9 Feb 2022

HAL is a multi-disciplinary open access archive for the deposit and dissemination of scientific research documents, whether they are published or not. The documents may come from teaching and research institutions in France or abroad, or from public or private research centers.

L'archive ouverte pluridisciplinaire **HAL**, est destinée au dépôt et à la diffusion de documents scientifiques de niveau recherche, publiés ou non, émanant des établissements d'enseignement et de recherche français ou étrangers, des laboratoires publics ou privés.

Glass formation and devitrification behavior of alkali (Li, Na) aluminosilicate melts containing TiO₂

Alessio Zandonà^{1,*}, Sandra Ory¹, Cécile Genevois¹, Emmanuel Véron¹, Aurélien Canizarès¹, Michael J. Pitcher¹, Mathieu Allix¹

¹CNRS, CEMHTI UPR3079, Univ. Orléans, F-45071 Orléans, France

Abstract

The impact of TiO₂ additions on the quenchability of melts derived from the stoichiometry of spodumene (LiAlSi₂O₆), eucryptite (LiAlSiO₄) and nepheline (NaAlSiO₄) was investigated by containerless melting. The results reveal a compositional dependence (Al₂O₃/SiO₂ and M₂O/Al₂O₃ ratios, M = Na or Li) of the role of TiO₂ during devitrification. Amorphous samples incorporating up to 10 mol% TiO₂ could be produced, above which devitrification invariably took place. Interaction of TiO₂ with other glass components (such as Al₂O₃ and Na₂O in nepheline glass) perceivably reduced glass stability, while eucryptite and spodumene glasses appeared only affected to the extent to which nanosized TiO₂ polymorphs (TiO₂(B), anatase and rutile) served as heterogeneous nucleation sites for quartz solid solutions, in which we inferred a substantial incorporation of Ti⁴⁺. A reduction in SiO₂ content and a preference for peraluminous compositions stand out as viable compositional strategies to foster the glass-forming ability of TiO₂-rich aluminosilicate melts.

Keywords: glass stability, glass-forming ability, glass-ceramics, TiO₂, quartz solid solutions

Corresponding author: Alessio Zandonà, alessio.zandona@cnrs-orleans.fr

1. Introduction

Controlled glass crystallization is a key stage in the production of glass-ceramics. It is most typically achieved through the addition of nucleating agents (or seed formers) [1] which favor homogeneous volume nucleation over unrestrained surface devitrification. Among such additives, TiO₂ represents one of the most versatile in aluminosilicate matrices: as a single seed former or in combination with ZrO₂, it enables the production of a number of technologically relevant materials, including high-strength cordierite and spinel glass-ceramics and low-thermal expansion glass-ceramics based on quartz solid solutions (Qss) [2–4]. Despite being investigated since the early days of glass-ceramic development [5], however, the fundamental laws controlling the nucleation efficiency of TiO₂ in different

compositional systems are still not fully understood: while 4 mol% are more than sufficient to induce volume crystallization in lithium aluminosilicate glass-ceramics (LAS) [6], higher additions (6-10 mol%) have been shown to be necessary in magnesium aluminosilicate (MAS) [7], sodium aluminosilicate (NAS) [8] and other multicomponent glasses [9–13]; conversely, TiO₂ was found to detrimentally foster surface nucleation in calcium aluminosilicate matrices [14]. The steady improvement of our analytical capabilities has recently shed new light on the complexity of seed formation, particularly within the LAS and MAS systems: (i) incipient liquid-liquid phase separation [15], (ii) a coupled increase in average coordination number of Ti and Al during crystal nucleation [16–18], (iii) the resulting pervasive nanostructural heterogeneity of the residual amorphous matrix [19,20] and (iv) the occurrence of TiO₂(B) as a metastable precursor to the formation of anatase and rutile [21,22] represent only some of the crucial phenomena involved in TiO₂ nucleation which were disentangled in the past few years.

In the wake of these works, we aimed at reinvestigating the compositional factors governing the successful homogeneous incorporation of TiO₂ into an amorphous aluminosilicate matrix, which is a basic prerequisite for the subsequent controlled crystallization of classical glass-ceramics. We selected containerless melting as the synthesis method due to its minimization of heterogeneous surface nucleation, which was shown to facilitate quenching of poor glass formers [23,24]. In this study, it particularly allowed to focus on the tendency of TiO₂-bearing crystals to precipitate homogeneously during quenching, obtaining a deeper insight into the specific influence of this seed former on the glass formation and devitrification behavior of alkali aluminosilicate melts. Our results are expected to assist the future compositional design of glass-ceramics, in which TiO₂ may play the role of a nucleating agent or, in turn, of the main functional component, as in glass-ceramic photocatalysts [25].

2. Experimental

Table 1 – Nominal melt compositions (mol%) examined within this work to investigate the glass-forming ability of alkali aluminosilicate melts and the devitrification behavior of the corresponding glasses doped with TiO₂ (M = Li or Na); liquidus temperatures T_m of the TiO₂-free compositions are reported from literature [26,27].

Sample	Li ₂ O	Na ₂ O	Al ₂ O ₃	SiO ₂	(M ₂ O)/Al ₂ O ₃	Al ₂ O ₃ /SiO ₂	T _m (K)
L1	25.0	-	25.0	50.0	1	0.5	1711 [26]
L1Li	33.3	-	16.7	50.0	2	0.33	1525 [26]
L1Al	16.7	-	33.3	50.0	0.5	0.66	1900 [26]
N1	-	25.0	25.0	50.0	1	0.5	1799 [27]
L2	16.7	-	16.7	66.6	1	0.25	1696 [26]

2.1 Synthesis of the samples

The starting compositions for this study (Fig. 1-a) corresponded to those of the minerals eucryptite (sample L1, LiAlSiO₄), spodumene (sample L2, LiAlSi₂O₆) and nepheline (sample N1, NaAlSiO₄). From the composition of L1, two additional glasses were obtained by keeping the SiO₂ content constant and modifying the Li₂O/Al₂O₃ molar ratio (respectively equal to 1 for L1, 2 for L1Li, 0.5 for L1Al). These five glass matrices were subsequently doped with increasing amounts of TiO₂ (up to 30 mol% in N1 and 20 mol% in the other glasses) to evaluate the influence of these additions on the glass-forming ability and devitrification behavior of the melts. The chosen nomenclature reflected these relations (e.g. L1LiT10 for 10 mol% TiO₂ + 90 mol% L1Li glass).

All samples were synthesized by aerodynamic levitation coupled to CO₂ laser heating (ADL); the experimental setup has been described elsewhere [28]. Laboratory-grade Li₂CO₃ (99%, Aldrich), Na₂CO₃ (99.5+%, Strem Chemicals) SiO₂ (99.999%, Strem Chemicals), Al₂O₃ (99.999%, Strem Chemicals) and TiO₂ (99.5%, Evonik P25) were thoroughly mixed in a hand mortar with the help of some ethanol and pressed into pellets of 1 g. Small chunks of these pellets were then melted by ADL in an O₂ flow, increasing the laser power until achieving a fully liquid spherical droplet. The maximum temperature was invariably below 1850 °C (in absence of a precise temperature calibration based on the composition-dependent thermal emittance of each sample, the temperature uncertainty is estimated as ± 100 °C of the pyrometer reading); after keeping it ~5 s, quenching was achieved by instantaneously switching off the lasers. The average quenching rate typically ranged between 200 and 400 K s⁻¹, depending on the bead size (Fig. 1-b). No appreciable evaporation of chemical components could be noticed during the whole

procedure: when tested, the final mass of the beads invariably corresponded to > 98.5% of the expected one after decarbonation.

All samples were examined directly in their as-quenched state. However, undoped L1 was additionally crystallized by treating some powdered glass at 900 °C for 2 h (estimated from DSC measurement) in air in a laboratory furnace (sample name: L1treated) or directly devitrified during the ADL synthesis, intentionally destabilizing the gas flow and letting the melt droplet bounce repeatedly on the nozzle walls to induce heterogeneous nucleation (sample name: L1dev). These two samples were used as references for the lattice parameters of TiO₂-free β-eucryptite.

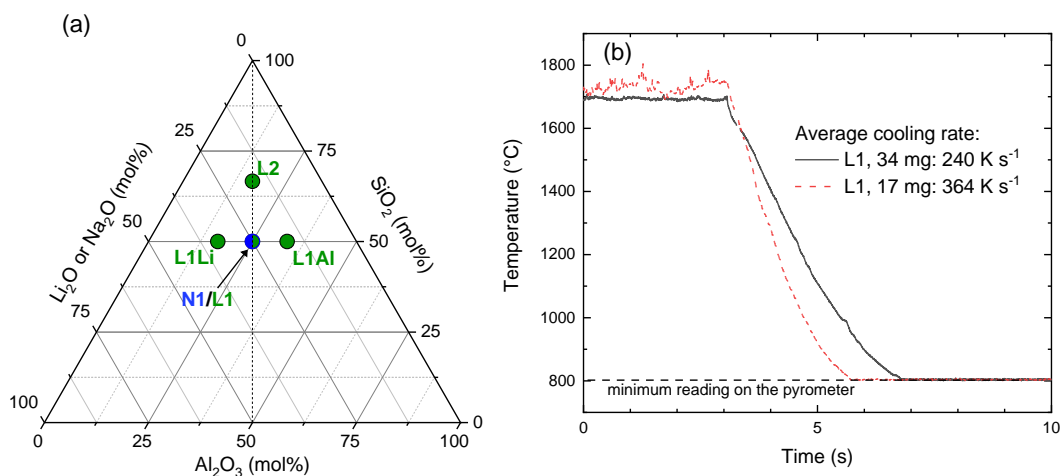


Figure 1. a) Ternary diagram of the system Li₂O (or Na₂O) – Al₂O₃ – SiO₂, locating the composition of the five base glasses analyzed within this work. b) Cooling curves obtained from the pyrometer readings during quenching in O₂ flow of beads of L1 composition with different masses; the absolute temperature uncertainty was estimated as ± 100 K of the reported values.

2.2 Raman spectroscopy

As-quenched beads were characterized at room temperature by Raman spectroscopy on a Renishaw InVia Qontor spectrometer mounting a green laser (514 nm) operated at 50 mW, although the power was occasionally reduced to avoid detector saturation in highly crystalline samples. The signal was collected in the range 80-2000 cm⁻¹ (low-wavenumber cutoff of the edge filter: ~100 cm⁻¹) using a 1800 lines/mm holographic grating, with 15 s acquisition time and 6 repetitions. Only visually homogeneous, not fully opaque samples were measured, focusing 20-40 μm below the surface with a 50x objective and acquiring spectra from several beads/locations to ensure reproducibility.

2.3 Differential scanning calorimetry (DSC)

Several beads of each composition were crushed to obtain 300 mg of coarse powder, which was measured in a platinum crucible on a SETARAM Multi HTC 1600, running a simple upscan at 10 K min^{-1} up to $1000 \text{ }^\circ\text{C}$. The instrument was calibrated based on the melting temperatures of several metallic standards (Al at $660 \text{ }^\circ\text{C}$, Ag at $962 \text{ }^\circ\text{C}$, Au at $1064 \text{ }^\circ\text{C}$), with an operational reproducibility of $\pm 1 \text{ K}$.

The obtained curves were processed to extract the glass transition midpoint T_g (double-tangent method) and the maxima of the exothermic events T_x (weak broad peak assigned to seed formation in L1T05 and L2T05, see below) and T_c (most intense crystallization peak, in all samples); the estimated uncertainty associated with these temperatures is preventively set at $\pm 5 \text{ K}$. These values were employed to derive glass stability as:

$$GS_x = T_x - T_g \quad (1)$$

or

$$GS_c = T_c - T_g \quad (2)$$

Glass-forming ability (*GFA*) was previously shown to be satisfactorily estimated through the Hrùby parameter [29,30]:

$$GFA = \frac{T_c - T_g}{T_m - T_c} \quad (3)$$

We calculated *GFA* for all undoped parent glasses, whose liquidus temperatures T_m (Tab. 1) could reliably be obtained from previous literature sources [26,27].

2.4 Powder X-ray diffraction (PXRD)

The crystalline assemblages of the samples with $\text{TiO}_2 \geq 10 \text{ mol}\%$ were determined by powder X-ray diffraction (PXRD) on a D8 Advance Bruker laboratory diffractometer (Bragg-Brentano geometry, $\text{Cu K}\alpha_{1,2}$ incident radiation, LynxEye XE line detector). The powder obtained from crushing and grinding single beads was dispersed on flat low-background Si sample holders and measured adjusting stepsize and acquisition time to the crystallinity of the sample. The lattice parameters of quartz solid solutions were obtained by Le-Bail fits using the software HighScore Plus (Panalytical); uncertainties were approximated by multiplying by three the estimated standard deviations (ESD) computed by the program.

2.5 Transmission electron microscopy (TEM)

Sample imaging and selected area electron diffraction (SAED) were performed with a Philips CM20 TEM operating at 200 kV . First, the beads were crushed in an agate mortar and dispersed in ethanol, then a drop of the mixture was loaded on copper grids layered by an amorphous holey carbon film.

3. Results

TiO₂-free references and samples containing 5 mol% TiO₂ could be easily quenched as glasses, as confirmed by the corresponding Raman spectra (Fig. 2) and parallel PXRD measurements (not shown for brevity). The data obtained from L1, L2 and N1 are in good agreement with previous experimental results [21,31], including the sharper appearance of the features between 400 and 600 cm⁻¹ in nepheline glass (N1) with respect to spodumene (L2) and eucryptite (L1). Similarly, the series L1Al – L1 – L1Li exhibited a coherent evolution, particularly evident in the progressive downshift and growth of the high-wavenumber envelope with increasing Li₂O content, manifesting a gradual structural depolymerization; a similar trend has been previously inferred from the Raman spectra of glasses belonging to the nepheline – diopside (NaAlSiO₄ – CaMgSi₂O₆) compositional series [32]. The addition of 5 mol% TiO₂ brought about a visible broadening of the vibrational features observed in the TiO₂-free glasses, as previously reported by other authors in nepheline glass [33]. Moreover, the emergence of an intense Raman band in the range 800-1000 cm⁻¹ could be noticed in L1T05, L1LiT05, L2T05 and N1T05, in agreement with previous works on TiO₂-doped spodumene and nepheline glasses [21,33]; similar bands are known to arise in SiO₂-TiO₂ glasses and have been interpreted as the signature for the incorporation of Ti⁴⁺ into the amorphous silicate network (e.g. in references [34–36]). In the case of sample L1AlT05, the broadening of the Raman spectrum was more prominent and, despite a clear rise in intensity at high wavenumber, no band specifically related to TiO₂ addition could be discerned.

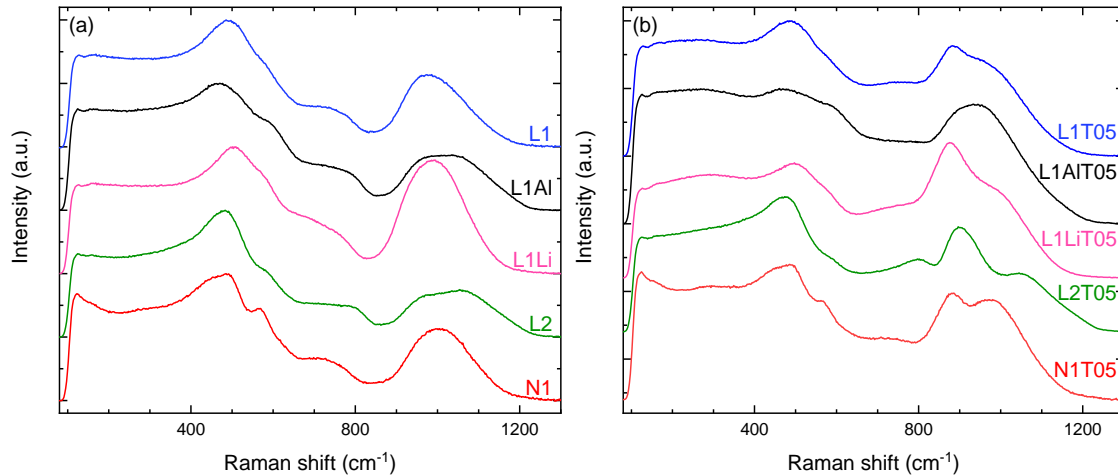


Figure 2. Raman spectra obtained from the as-quenched samples: a) without TiO₂ addition and b) with 5 mol% TiO₂.

The addition of 5 mol% TiO₂ had also a substantial impact on the response of the glasses to a secondary heat treatment, as revealed by DSC upscans at 10 K min⁻¹ (Fig. 3): (i) glass transition and crystallization shifted to lower temperatures in L1T05, L2T05, N1T05 and L1AlT05 as compared to their TiO₂-free references (similar observations have been reported in other TiO₂-doped aluminosilicate glasses [19,20,37,38]); (ii) in L1LiT05, the glass transition and crystallization onset appeared instead slightly higher than in L1Li; (iii) the main crystallization event exhibited a remarkable sharpening in L1T05, L2T05 and L1LiT05 as compared to their TiO₂-free references; (iii) as previously noticed in similar aluminosilicate glasses and ascribed to the formation of TiO₂-containing seeds [19], the strongest crystallization peak of L1T05 and L2T05 was preceded by a broader and less intense exothermic maximum (T_x). From these results, glass forming ability GFA and glass stability GS_c and GS_x parameters were calculated as defined in Section 2.3. Among the TiO₂-free glasses, L2 and N1 exhibited the highest glass-forming ability and glass stability, whereas L1 was found to be the least stable. Upon TiO₂ doping, the GS_c parameter of the parent glasses was significantly lowered only in L1LiT05 (from 105 K to 85 K) and N1T05 (from 158 K to 116 K). Nevertheless, L1T05 and L2T05 resulted the least stable glasses if GS_x was considered, with respective values of 60 K and 79 K.

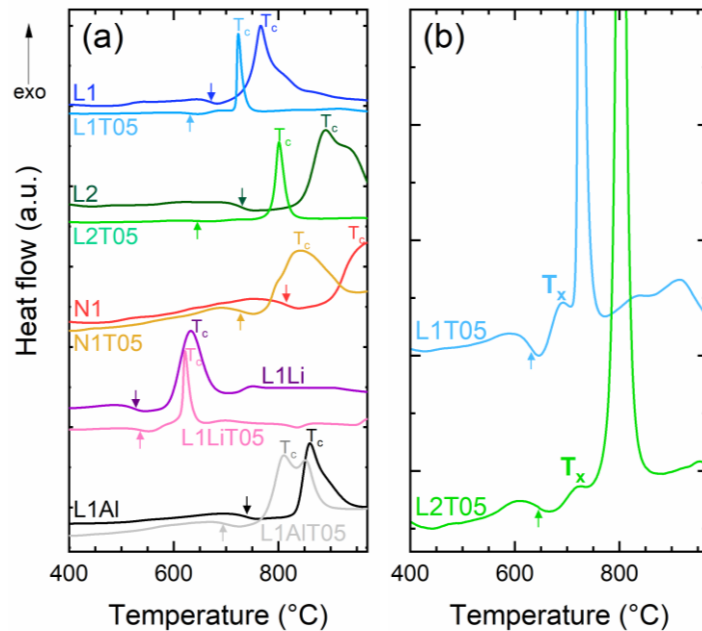


Figure 3. a) DSC traces obtained from samples doped with 5 mol% TiO₂, in comparison to their undoped base glasses (an arrow indicates the glass transition midpoint T_g , T_c labels the most intense crystallization peak); b) excerpt of the DSC curves of L1T05 and L2T05, highlighting the weak exothermic peak (T_x) associated to the precipitation of TiO₂-bearing crystals [19].

Table 2. Characteristic temperatures for the glass transition midpoint (T_g), main crystallization peak (T_c) and TiO₂-related seed formation (T_x) extracted from DSC measurements (estimated uncertainty = ± 5 K) of all base compositions studied within this work, both undoped and with 5 mol% TiO₂. These temperatures were used to compute glass-forming ability (GFA) and glass stability (GS_c and GS_x) as defined in Section 2.3.

Composition	0 mol% TiO ₂				5 mol% TiO ₂				
	T_g (K)	T_c (K)	GS_c (K)	GFA	T_g (K)	T_c (K)	T_x (K)	GS_c (K)	GS_x (K)
L1	945	1039	94	0.14	905	996	965	91	60
L2	1004	1163	159	0.30	919	1074	998	155	79
N1	1087	1245	158	0.29	1000	1116	-	116	-
L1Li	801	906	105	0.17	809	894	-	85	-
L1Al	1012	1133	121	0.16	967	1084	-	117	-

Raman spectroscopy and PXRD were combined to identify the formation of crystalline phases or to verify the amorphous state of samples containing TiO₂ amounts ≥ 10 mol% (Figs. 4 and 5). While sample L1T10 was still amorphous, L1T15 and L1T20 completely crystallized into a Qss phase exhibiting the typical superstructural features of β -eucryptite [39]. Alongside this phase, the Raman spectrum of L1T15 clearly revealed the presence of anatase, while L1T20 contained rutile according to PXRD. Interpretation of the broad Raman spectra of L1Al-based samples proved rather challenging, but PXRD clarified that a slight devitrification occurred in L1AlT15 with the appearance of broad reflections of difficult assignment, while L1AlT20 showed peaks univocally assignable to Qss and rutile. L1LiT10, L1LiT15 and L1LiT20 contained instead Li-titanate phases [40] in a still amorphous aluminosilicate matrix. In agreement with previous experimental results [21], L2T10 developed a mixture of nanocrystalline anatase and TiO₂(B), whereas L2T15 and L2T20 marked the appearance of rutile and the devitrification of the aluminosilicate matrix into Qss (no visible superstructure, as expected for a spodumene stoichiometry [39]) and keatite solid solution (Kss). Finally, while N1T10 was still amorphous, the Raman spectra of N1T15 and N1T20 definitely revealed the formation of a phase similar to TiO₂(B), indexable as a Na- and Al-bearing titanate bronze by PXRD [41] and accompanied by rutile in N1T30. Nanostructural checks performed by TEM (Fig. 6 and supplementary material) corroborated the above-presented results.

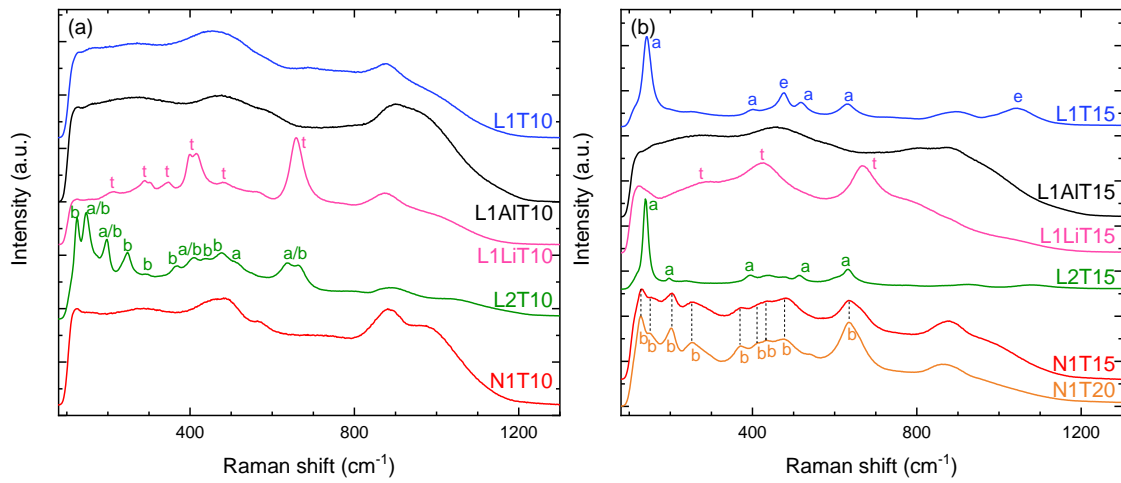


Figure 4. Raman spectra obtained from the as-quenched samples, containing a) 10 mol% TiO₂ and b) 15 mol% TiO₂; the spectrum of N1T20 is also reported due to the still low crystallinity of N1T15 (*a* for anatase, *b* for TiO₂-bronze, *e* for β-eucryptite, *t* for cubic Li-titanate).

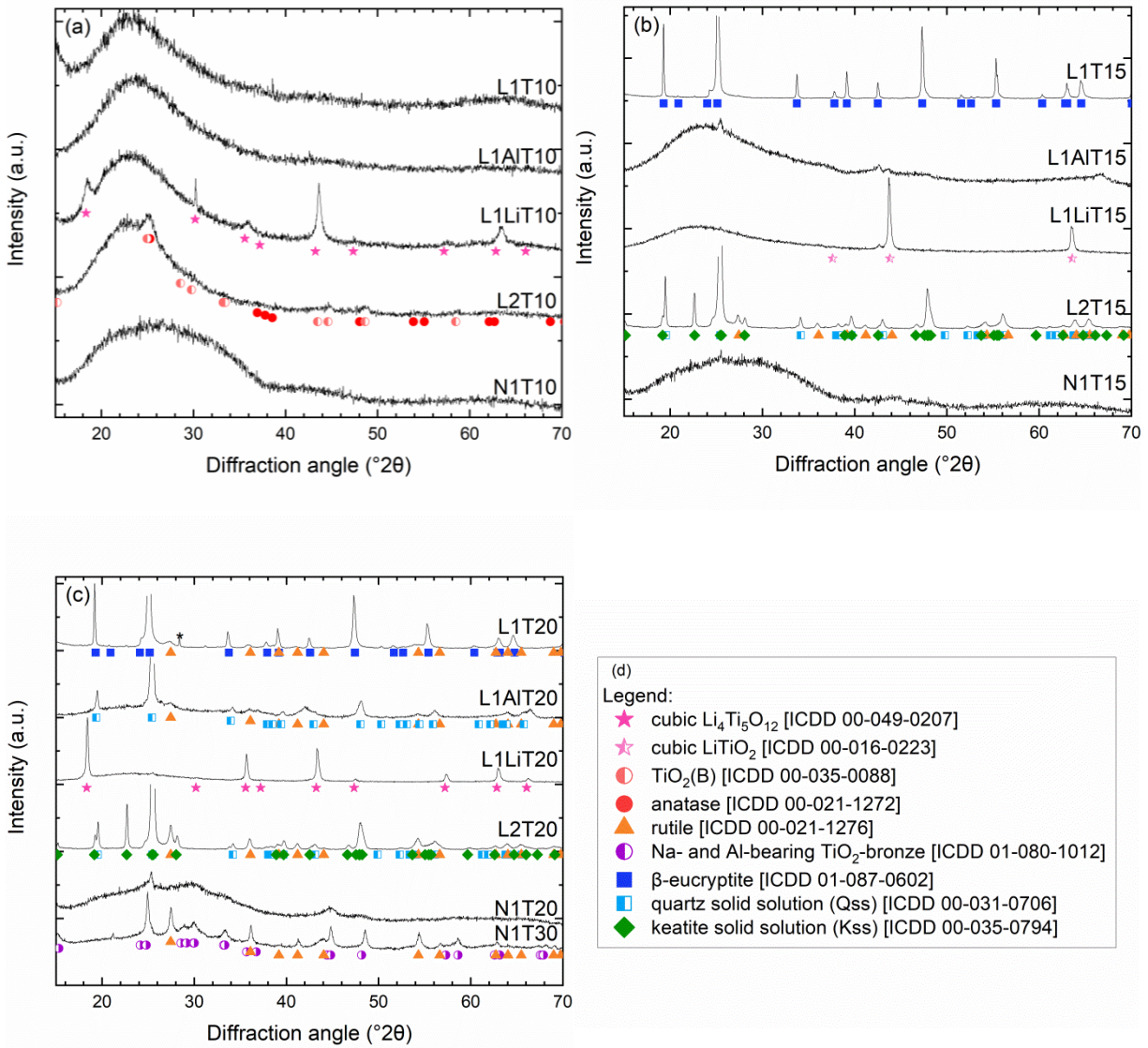


Figure 5. X-ray diffraction patterns obtained from as-quenched samples, containing a) 10 mol%, b) 15 mol% and c) 20 mol% TiO₂; d) legend associating all symbols to the reference patterns used for indexation (* for Si sample holder).

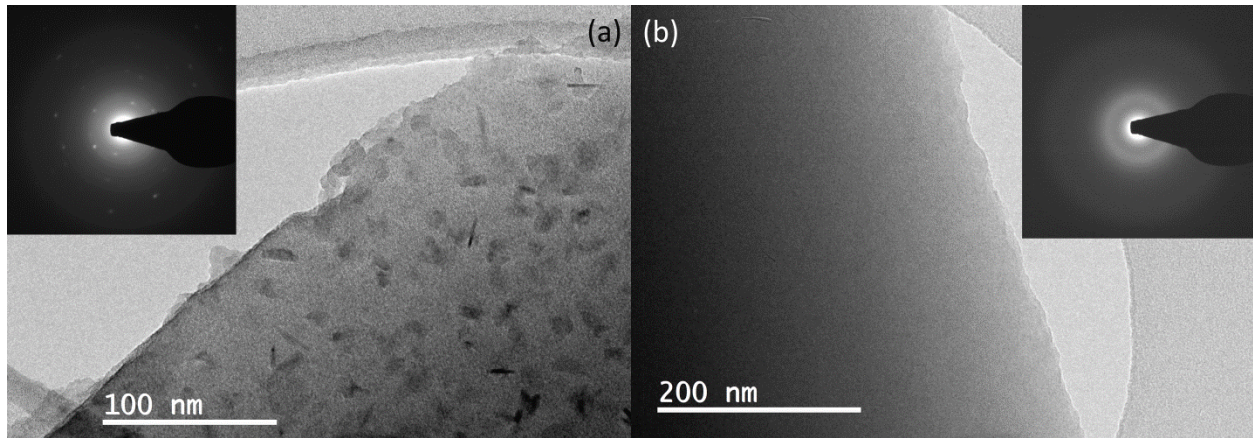


Figure 6. Bright-field TEM images and SAED patterns (inlets) of as-quenched samples: a) L2T10, exhibiting dark crystallites and visible diffraction spots; b) L1AlT10, appearing homogeneous and amorphous. Mind the slightly different magnification, scale bars are provided.

The lattice parameters of Qss phases obtained in L1- and L2-based samples were compared to the available literature sources (Qss synthesis respectively by: glass crystallization [42,43], high-temperature sintering or high-temperature high-pressure processing [39], melt growth from a fluorinated flux [44]) to identify possible variations from an ideal stoichiometry (Fig. 7). In agreement with these sources, the weak superstructure peaks (*a*- and *c*- doubling) in samples with eucryptite stoichiometry (L1) were disregarded and only the smaller cell of Qss was refined, to simultaneously examine the whole compositional range. Literature values exhibit a general agreement but scatter over a relatively wide range at the stoichiometry of eucryptite ($\text{Al}_2\text{O}_3/\text{SiO}_2$ ratio = 0.5), possibly manifesting the various synthesis methods and the resulting different ordering states achievable in the tetrahedral sites (Al-Si) and at Li channel positions. Indeed, our TiO_2 -free references (L1dev and L1treated) matched well with the values of authors employing glass crystallization [42]. Qss crystals crystallized from TiO_2 -bearing melts exhibited instead remarkably higher lattice constants than the available references: this was evident for both *a* and *c* parameters at spodumene stoichiometry (L2-based samples) and particularly for the *a* parameter of eucryptite compositions (L1-based samples). Notice that the lattice parameters of Kss computed in L2-based samples (Tab. 1) invariably agreed very well with the available references [45,46].

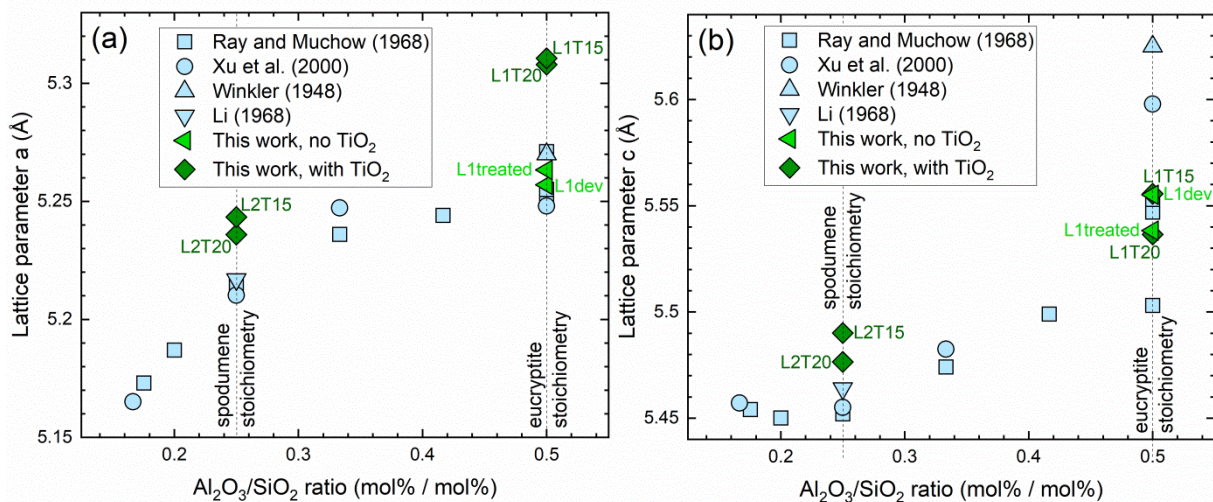


Figure 7. a) Lattice parameters a and b) lattice parameters c obtained for Qss phases in samples L1T15, L1T20, L2T15, L2T20, plotted according to the $\text{Al}_2\text{O}_3/\text{SiO}_2$ ratio of their parent glass and in comparison to our TiO_2 -free reference L1 (devitrified directly from the molten state (-dev) or crystallized from glass (-treated)) and to various literature sources [39,42–44]. Error bars are smaller than the depicted symbols.

Table 3. Lattice parameters obtained from PXRD measurement of Qss phases formed in samples of L1, L1T15, L1T20, L2T15 and L2T20 composition. Digits in parentheses provide the estimated uncertainties for the determined values.

Sample	Synthesis	Phase	Parameter	
			a (Å)	c (Å)
L1T15	Devitrified	Qss	5.3107(5)	5.5556(7)
L1T20	Devitrified	Qss	5.3079(7)	5.536(1)
L1	Devitrified	Qss	5.2571(4)	5.5551(7)
L1	Treated at 900°C for 2h	Qss	5.2633(3)	5.5383(6)
L2T15	Devitrified	Qss	5.243(3)	5.490(3)
L2T15	Devitrified	Kss	7.571(4)	9.166(6)
L2T20	Devitrified	Qss	5.236(6)	5.476(7)
L2T20	Devitrified	Kss	7.578(6)	9.15(1)

4. Discussion

The quenchability of homogeneous aluminosilicate glasses containing TiO_2 depends on a number of competing processes, which this study aimed to isolate and characterize. We selected five glass matrices that exhibited inherent dissimilarities in glass-forming ability, as manifested by the computation of their *GFA* parameters (Tab. 2). However, the use of containerless melting allowed us to level off these initial differences through the suppression of heterogeneous nucleation, to the point that even our least stable parent glass (L1) would not devitrify after several seconds spent at deep undercooling, if heterogeneous crystallization was not triggered artificially by a contact to the ADL nozzle (see also Section 2.1).

Table 4. Schematic summary of the devitrification behavior of the analyzed samples: for each TiO_2 content (mol%), *Ti* indicates the formation of (alumino)titanate phases and *Si* the formation of (alumino)silicate phases.

TiO_2 content (mol%)	L1	L2	N1	L1Li	L1Al
0	-	-	-	-	-
5	-	-	-	-	-
10	-	Ti	-	Ti	-
15	Ti + Si	Ti + Si	Ti	Ti	Ti + Si
20	Ti + Si	Ti + Si	Ti	Ti	Ti + Si

After the addition of a seed former, however, another phenomenon became crucial for the formation of crystals, i.e. a temperature-dependent TiO_2 oversaturation in the undercooled melts [47,48], leading to the homogeneous precipitation of Ti-bearing nuclei. As summarized in Table 4, TiO_2 was found to be retained in the amorphous structure of the samples only up to a certain threshold level, above which Ti-bearing crystalline phases could be invariably identified, with crystal sizes and shapes (Fig. 6 and supplementary material) that mostly resembled those classically obtainable during seed formation in glass-ceramics [15,18,19,21]. In other words, we can interpret most of these crystals as the product of low-temperature precipitation due to oversaturation during quenching, which could not be prevented despite the relatively fast cooling rate of our ADL system (roughly between 200 and 400 K s^{-1} , as shown in Fig. 1-b). All in all, a decrease in overall SiO_2 content and an enrichment in Al_2O_3 appear beneficial for the obtainment of homogeneous aluminosilicate glasses doped with TiO_2 , in agreement with recent results on ZrO_2 -bearing (magnesium) aluminosilicate glasses [28]. Our observations may indeed seem counterintuitive in the light of the available geochemical models [47,48], which predict higher solubility of TiO_2 in peralkaline melts at a given temperature. Nevertheless, the geochemical prediction of the

subliquidus equilibrium melt solubility for TiO_2 (or ZrO_2) differs conceptually from our investigation of the glass forming ability of melts containing TiO_2 (or ZrO_2).

Especially at the highest TiO_2 contents (20 mol%), however, the possible formation of a TiO_2 -enriched liquid phase due to stable (superliquidus) immiscibility should be taken into account, since a liquid-liquid immiscibility field is known to exist in the SiO_2 - TiO_2 system [49] and would necessarily subvert the overall devitrification mechanism. The formation of TiO_2 -enriched liquid droplets, for instance, could be compatible with the rounded grain shapes observed in samples belonging to the L1Li-series (Figs. S4, S5 and S6), although the experimental in-situ verification of this occurrence at temperatures above 1300 °C implies undeniable analytical challenges.

Furthermore, the presence (or absence) of aluminosilicate phases in the quenched beads still shows to be directly influenced by the behavior of TiO_2 . Samples belonging to the N1- and L1Li-series developed Ti-bearing crystals which also incorporated other glass components (Li_2O , Na_2O , Al_2O_3); it is therefore likely that the residual SiO_2 -enriched matrix eventually exhibited an enhanced glass-forming ability, which prevented it from devitrification. In the case of the L1- and L2-series, instead, the precipitation of TiO_2 nanocrystals provided new sites for heterogeneous nucleation in a residual melt still very close to its parent composition, triggering the formation of Qss and Kss. Phase selection during devitrification among metastable ($\text{TiO}_2(\text{B})$ and anatase) and stable TiO_2 polymorphs (rutile) was previously shown to obey Ostwald's rule of stages [50], according to which less dense and less symmetric phases may be kinetically favored during precipitation from the amorphous structure of an aluminosilicate melt. Moreover, the occurrence of $\text{TiO}_2(\text{B})$ in SiO_2 - TiO_2 glass-ceramics [22] could be correlated to a particularly high surface-to-volume ratio of the crystals, which would also apply to the TiO_2 nanoplatelets observed in this work (Figure 6-a) and in previous studies [21]; a similar mechanism is assumed to be responsible for the stabilization of anatase over rutile at small crystallite sizes [51].

The remarkably high values of the lattice parameters obtained for Qss convincingly suggest a partial incorporation of Ti^{4+} (effective ionic radius = 0.42 Å, while Al^{3+} = 0.39 Å and Si^{4+} = 0.26 Å [52]) in their structure, possibly originating from that fraction of TiO_2 still dissolved in the aluminosilicate melt at the temperature of devitrification. Regrettably, the overlap of the main diffraction peaks of Qss (or β -eucryptite) and anatase and the nanosize of this latter phase prevented a reliable quantification of the TiO_2 crystalline fraction by Rietveld refinements. Nevertheless, TiO_2 incorporation in the structure of cristobalite was similarly identified by other authors upon high-temperature devitrification [53], possibly because in such condition the rate of crystal growth can overtake that of TiO_2 homogeneous nucleation. As for the samples of L1Al-basis, they appeared to undergo more complex devitrification reactions, also considering the intricate nanostructure of L1AlT15 (Fig. S3 in the supplementary material). The affinity between Ti^{4+} and Al^{3+} during phase separation and nucleation in the LAS system has been previously

reported by several authors [15,18,21,54] and is probably responsible for the atypical devitrification of these strongly peraluminous samples.

The contrasting behavior of different amorphous matrices after TiO_2 doping was analogously evident from the results of DSC measurements. L1AlT05 was the only sample whose glass stability appeared unaffected in comparison to its parent glass L1Al, suggesting an especially favorable incorporation of Ti^{4+} into its amorphous structure. On the other hand, the addition of TiO_2 clearly facilitated devitrification in L1LiT05 with respect to its undoped parent glass, despite the fact that T_g was virtually identical in both materials. This latter observation differs from the reduction of low-temperature viscosity usually detected in alkali peraluminous melts upon TiO_2 addition [19,20,37], possibly confirming the re-polymerizing role of this oxide previously suggested by other authors in aluminosilicate melts containing non-bridging oxygens [55]. The glass stability of L1T05 and L2T05, though seemingly unaffected as GS_c , was instead heavily reduced by the exothermic event T_x assigned to the formation of TiO_2 seeds, as expectable from the known nucleating efficiency of this oxide in LAS glass-ceramics [21]. As for N1T05, TiO_2 clearly did not behave as a classically defined seed former: it interacted with the other glass components, deeply impacting glass stability and crystallization sequence.

5. Conclusion

The results of our study highlight the complex influence of TiO_2 on the glass-forming ability and devitrification behavior of aluminosilicate melts, providing further evidence that seed formers cannot be considered as simple chemically-inert additions to the glass. We have shown that, depending on composition, TiO_2 can certainly foster heterogeneous nucleation (e.g. in spodumene and eucryptite glasses upon secondary annealing) but also be partially integrated into the crystalline structure of aluminosilicate phases (e.g. in spodumene and eucryptite melts undergoing high-temperature devitrification). Alternatively, TiO_2 can combine with other glass components and heavily affect the devitrification sequence through the formation of titanate phases (as observed in nepheline melts and in peralkaline matrices). Both reducing SiO_2 content and moving towards peraluminous compositions appear to be viable compositional strategies to maximize TiO_2 incorporation in homogeneous aluminosilicate glasses.

Acknowledgements

Alessio Zandonà wishes to acknowledge the Deutsche Forschungsgemeinschaft (DFG) for funding his research through the Walter Benjamin Program, grant n. ZA 1188/1-1. The authors are grateful to the ICMN laboratory (Orléans, France) for TEM access and to the French Agency for

Research (Agence Nationale de la Recherche, ANR) for its financial support through the Equipex Planex ANR-11-EQPX-36.

References

- [1] J. Deubener, M. Allix, M.J. Davis, A. Duran, T. Höche, T. Honma, T. Komatsu, S. Krüger, I. Mitra, R. Müller, S. Nakane, M.J. Pascual, J.W.P. Schmelzer, E.D. Zanotto, S. Zhou, Updated definition of glass-ceramics, *Journal of Non-Crystalline Solids*. 501 (2018) 3–10. <https://doi.org/10.1016/j.jnoncrysol.2018.01.033>.
- [2] G.H. Beall, Design and Properties of Glass-Ceramics, *Annual Review of Materials Science*. 22 (1992) 91–119. <https://doi.org/10.1146/annurev.ms.22.080192.000515>.
- [3] L.R. Pinckney, Transparent, high strain point spinel glass-ceramics, *Journal of Non-Crystalline Solids*. 255 (1999) 171–177. [https://doi.org/10.1016/S0022-3093\(99\)00368-3](https://doi.org/10.1016/S0022-3093(99)00368-3).
- [4] D. Krause, H. Bach, eds., *Low Thermal expansion Glass Ceramics*, Springer Berlin Heidelberg, 2005.
- [5] S.D. Stookey, Catalyzed Crystallization of Glass in Theory and Practice, *Ind. Eng. Chem.* 51 (1959) 805–808. <https://doi.org/10.1021/ie50595a022>.
- [6] T.I. Barry, L.A. Lay, R.P. Miller, Nucleation efficiency in lithia-alumina-silica glasses, *Discuss. Faraday Soc.* 50 (1970) 214–221. <https://doi.org/10.1039/DF9705000214>.
- [7] A.G. Gregory, T.J. Veasey, The crystallisation of cordierite glass, *Journal of Materials Science*. 6 (1971) 1312–1321. <https://doi.org/10.1007/BF00552045>.
- [8] D.A. Duke, J.F. MacDowell, B.R. Karstetter, Crystallization and Chemical Strengthening of Nepheline Glass-Ceramics, *Journal of the American Ceramic Society*. 50 (1967) 67–74. <https://doi.org/10.1111/j.1151-2916.1967.tb15041.x>.
- [9] A. Zandona, B. Rüdinger, O. Hochrein, J. Deubener, Crystallization sequence within the keatite solid solution – cordierite mixed compositional triangle with TiO₂ as nucleating agent, *Journal of Non-Crystalline Solids*. 505 (2019) 320–332. <https://doi.org/10.1016/j.jnoncrysol.2018.11.012>.
- [10] M. Ma, W. Ni, Y. Wang, Z. Wang, F. Liu, The effect of TiO₂ on phase separation and crystallization of glass-ceramics in CaO–MgO–Al₂O₃–SiO₂–Na₂O system, *Journal of Non-Crystalline Solids*. 354 (2008) 5395–5401. <https://doi.org/10.1016/j.jnoncrysol.2008.09.019>.
- [11] G.A. Khater, M.H. Idris, Role of TiO₂ and ZrO₂ on crystallizing phases and microstructure in Li, Ba aluminosilicate glass, *Ceramics International*. 33 (2007) 233–238. <https://doi.org/10.1016/j.ceramint.2005.08.016>.
- [12] H. Kim, W. Choi, Surface and bulk crystallization in Nd₂O₃–Al₂O₃–SiO₂–TiO₂ glasses, *Journal of the European Ceramic Society*. 24 (2004) 2103–2111. [https://doi.org/10.1016/S0955-2219\(03\)00357-1](https://doi.org/10.1016/S0955-2219(03)00357-1).
- [13] L. Barbieri, A.B. Corradi, C. Leonelli, C. Siligardi, T. Manfredini, G.C. Pellacani, Effect of TiO₂ addition on the properties of complex aluminosilicate glasses and glass-ceramics, *Materials Research Bulletin*. 32 (1997) 637–648. [https://doi.org/10.1016/S0025-5408\(97\)00029-9](https://doi.org/10.1016/S0025-5408(97)00029-9).
- [14] R.-G. Duan, K.-M. Liang, S.-R. Gu, Effect of changing TiO₂ content on structure and crystallization of CaO–Al₂O₃–SiO₃ system glasses, *Journal of the European Ceramic Society*. 18 (1998) 1729–1735. [https://doi.org/10.1016/S0955-2219\(98\)00105-8](https://doi.org/10.1016/S0955-2219(98)00105-8).
- [15] E. Kleebusch, C. Patzig, T. Höche, C. Rüssel, The evidence of phase separation droplets in the crystallization process of a Li₂O–Al₂O₃–SiO₂ glass with TiO₂ as nucleating agent – An X-ray diffraction and (S)TEM-study supported by EDX-analysis, *Ceramics International*. 44 (2018) 2919–2926. <https://doi.org/10.1016/j.ceramint.2017.11.040>.
- [16] L. Cormier, O. Dargaud, N. Menguy, G.S. Henderson, M. Guignard, N. Trcera, B. Watts, Investigation of the Role of Nucleating Agents in MgO–SiO₂–Al₂O₃–SiO₂–TiO₂ Glasses and Glass-Ceramics: A XANES Study at the Ti K- and L_{2,3}-Edges, *Crystal Growth & Design*. 11 (2011) 311–319. <https://doi.org/10.1021/cg101318p>.

- [17] M. Guignard, L. Cormier, V. Montouillout, N. Menguy, D. Massiot, A.C. Hannon, B. Beuneu, Rearrangement of the structure during nucleation of a cordierite glass doped with TiO₂, *Journal of Physics: Condensed Matter*. 22 (2010) 185401. <https://doi.org/10.1088/0953-8984/22/18/185401>.
- [18] E. Kleebusch, C. Patzig, M. Krause, Y. Hu, T. Höche, C. Rüssel, The effect of TiO₂ on nucleation and crystallization of a Li₂O-Al₂O₃-SiO₂ glass investigated by XANES and STEM, *Scientific Reports*. 8 (2018) 2929. <https://doi.org/10.1038/s41598-018-21227-x>.
- [19] A. Zandona, C.B.M. Groß, B. Rüdinger, J. Deubener, A threshold heating rate for single-stage heat treatments in glass-ceramics containing seed formers, *Journal of the American Ceramic Society*. n/a (2021). <https://doi.org/10.1111/jace.17822>.
- [20] D. Di Genova, A. Zandona, J. Deubener, Unravelling the effect of nano-heterogeneity on the viscosity of silicate melts: Implications for glass manufacturing and volcanic eruptions, *Journal of Non-Crystalline Solids*. 545 (2020) 120248. <https://doi.org/10.1016/j.jnoncrysol.2020.120248>.
- [21] A. Zandona, C. Patzig, B. Rüdinger, O. Hochrein, J. Deubener, TiO₂(B) nanocrystals in Ti-doped lithium aluminosilicate glasses, *Journal of Non-Crystalline Solids: X*. 2 (2019) 100025. <https://doi.org/10.1016/j.nocx.2019.100025>.
- [22] A. Zandona, A. Martínez Arias, M. Gutbrod, G. Hensch, A.P. Weber, J. Deubener, Spray-Dried TiO₂(B)-Containing Photocatalytic Glass-Ceramic Nanobeads, *Advanced Functional Materials*. 31 (2021) 2007760. <https://doi.org/10.1002/adfm.202007760>.
- [23] K. Yoshimoto, A. Masuno, H. Inoue, Y. Watanabe, Transparent and High Refractive Index La₂O₃-WO₃ Glass Prepared Using Containerless Processing, *Journal of the American Ceramic Society*. 95 (2012) 3501–3504. <https://doi.org/10.1111/j.1551-2916.2012.05439.x>.
- [24] Z. Mao, J. Duan, X. Zheng, M. Zhang, L. Zhang, H. Zhao, J. Yu, Study on optical properties of La₂O₃-TiO₂-Nb₂O₅ glasses prepared by containerless processing, *Ceramics International*. 41 (2015) S51–S56. <https://doi.org/10.1016/j.ceramint.2015.03.154>.
- [25] G. Singh, M. Sharma, R. Vaish, Emerging trends in glass-ceramic photocatalysts, *Chemical Engineering Journal*. 407 (2021) 126971. <https://doi.org/10.1016/j.cej.2020.126971>.
- [26] B. Konar, D.-G. Kim, I.-H. Jung, Critical thermodynamic optimization of the Li₂O-Al₂O₃-SiO₂ system and its application for the thermodynamic analysis of the glass-ceramics, *Journal of the European Ceramic Society*. 38 (2018) 3881–3904. <https://doi.org/10.1016/j.jeurceramsoc.2018.04.031>.
- [27] N.L. Bowen, J.F. Schairer, Crystallization Equilibrium in Nepheline-Albite-Silica Mixtures with Fayalite, *The Journal of Geology*. 46 (1938) 397–411.
- [28] A. Zandona, M. Moustros, C. Genevois, E. Véron, A. Canizarès, M. Allix, Glass-forming ability and ZrO₂ saturation limits in the magnesium aluminosilicate system, *Ceramics International*. (2021). <https://doi.org/10.1016/j.ceramint.2021.12.051>.
- [29] A. Hrubý, Evaluation of glass-forming tendency by means of DTA, *Czechoslovak Journal of Physics B*. 22 (1972) 1187–1193. <https://doi.org/10.1007/BF01690134>.
- [30] M.L.F. Nascimento, L.A. Souza, E.B. Ferreira, E.D. Zanotto, Can glass stability parameters infer glass forming ability?, *Journal of Non-Crystalline Solids*. 351 (2005) 3296–3308. <https://doi.org/10.1016/j.jnoncrysol.2005.08.013>.
- [31] J. Marcial, J. Kabel, M. Saleh, N. Washton, Y. Shaharyar, A. Goel, J.S. McCloy, Structural dependence of crystallization in glasses along the nepheline (NaAlSi₃O₈) - eucryptite (LiAlSi₂O₆) join, *Journal of the American Ceramic Society*. 101 (2018) 2840–2855. <https://doi.org/10.1111/jace.15439>.
- [32] D. Sykes, C.M. Scarfe, Melt structure in the system nepheline-dioptase, *Journal of Geophysical Research: Solid Earth*. 95 (1990) 15745–15749. <https://doi.org/10.1029/JB095iB10p15745>.
- [33] E.T. Nienhuis, J. Marcial, T. Robine, C. Le Losq, D.R. Neuville, M.C. Stennett, N.C. Hyatt, J.S. McCloy, Effect of Ti⁴⁺ on the structure of nepheline (NaAlSi₃O₈) glass, *Geochimica et Cosmochimica Acta*. 290 (2020) 333–351. <https://doi.org/10.1016/j.gca.2020.09.015>.
- [34] M.C. Tobin, T. Baak, Raman Spectra of Some Low-Expansion Glasses, *J. Opt. Soc. Am.* 58 (1968) 1459. <https://doi.org/10.1364/JOSA.58.001459>.

- [35] B.G. Varshal, V.N. Denisov, B.N. Mavrin, G.A. Parlova, V.B. Podobedov, Kh.E. Sterin, Spectra of Raman and hyper-Raman light scattering of the TiO₂-SiO₂ glass system, *Opt. Spektrosk.* 47 (1979) 619–622.
- [36] H.R. Chandrasekhar, M. Chandrasekhar, M.H. Manghnani, Phonons in TiO₂-SiO₂ glasses, *Journal of Non-Crystalline Solids.* 40 (1980) 567–575. [https://doi.org/10.1016/0022-3093\(80\)90130-1](https://doi.org/10.1016/0022-3093(80)90130-1).
- [37] Q. Fu, B.R. Wheaton, K.L. Geisinger, A.J. Credle, J. Wang, Crystallization, Microstructure, and Viscosity Evolutions in Lithium Aluminosilicate Glass-Ceramics, *Frontiers in Materials.* 3 (2016) 49. <https://doi.org/10.3389/fmats.2016.00049>.
- [38] E.T. Nienhuis, N.J. Smith-Gray, G.N. Cocking, J. Marcial, Y. Zhang, M. Ahmadzadeh, A. Goel, J.S. McCloy, A comparative study on the effect of Zr, Sn, and Ti on the crystallization behavior of nepheline glass, *Journal of Non-Crystalline Solids.* 569 (2021) 120970. <https://doi.org/10.1016/j.jnoncrysol.2021.120970>.
- [39] H. Xu, P.J. Heaney, G.H. Beall, Phase transitions induced by solid solution in stuffed derivatives of quartz: A powder synchrotron XRD study of the LiAlSiO₄-SiO₂ join, *American Mineralogist.* 85 (2000) 971–979. <https://doi.org/10.2138/am-2000-0711>.
- [40] D. Capsoni, M. Bini, V. Massarotti, P. Mustarelli, S. Ferrari, G. Chiodelli, M.C. Mozzati, P. Galinetto, Cr and Ni Doping of Li₄Ti₅O₁₂: Cation Distribution and Functional Properties, *J. Phys. Chem. C.* 113 (2009) 19664–19671. <https://doi.org/10.1021/jp906894v>.
- [41] H. Toraya, N. Masciocchi, W. Parrish, Rietveld powder structure refinement of Na₂Al₂Ti₆O₁₆; Comparison of synchrotron radiation and conventional x-ray tube datasets, *Journal of Materials Research.* 5 (1990) 1538–1543. <https://doi.org/10.1557/JMR.1990.1538>.
- [42] S. Ray, G.M. Muchow, High-Quartz Solid Solution Phases from Thermally Crystallized Glasses of Compositions Li₂O₂, MgO, Al₂O₃, nSiO₂, *Journal of the American Ceramic Society.* 51 (1968) 678–682. <https://doi.org/10.1111/j.1151-2916.1968.tb15927.x>.
- [43] C.-T. Li, The crystal structure of LiAlSi₂O₆ III (high-quartz solid solution), *Zeitschrift Für Kristallographie - Crystalline Materials.* 127 (1968) 327–348. <https://doi.org/doi:10.1524/zkri.1968.127.16.327>.
- [44] H.G.F. Winkler, Synthese und Kristallstruktur des Eukryptits, LiAlSiO₄, *Acta Crystallographica.* 1 (1948) 27–34. <https://doi.org/10.1107/S0365110X48000065>.
- [45] W. Ostertag, G.R. Fischer, J.P. Williams, Thermal Expansion of Synthetic β-Spodumene and β-Spodumene—Silica Solid Solutions, *Journal of the American Ceramic Society.* 51 (1968) 651–654. <https://doi.org/10.1111/j.1151-2916.1968.tb12638.x>.
- [46] B.J. Skinner, H.T. Evans, Crystal chemistry of β-spodumene solid solutions on the join Li₂O.Al₂O₃-SiO₂, *Am. J. Sci.* 258 (1960) 312–324.
- [47] F.J. Ryerson, E.B. Watson, Rutile saturation in magmas: implications for TiNbTa depletion in island-arc basalts, *Earth and Planetary Science Letters.* 86 (1987) 225–239. [https://doi.org/10.1016/0012-821X\(87\)90223-8](https://doi.org/10.1016/0012-821X(87)90223-8).
- [48] G.A. Gaetani, P.D. Asimow, E.M. Stolper, A model for rutile saturation in silicate melts with applications to eclogite partial melting in subduction zones and mantle plumes, *Earth and Planetary Science Letters.* 272 (2008) 720–729. <https://doi.org/10.1016/j.epsl.2008.06.002>.
- [49] R.C. DeVries, R. Roy, E.F. Osborn, Phase Equilibria in the System CaO-TiO₂-SiO₂, *Journal of The American Ceramic Society.* 38 (1955) 158–171.
- [50] W. Ostwald, Studien über die Bildung und Umwandlung fester Körper: 1. Abhandlung: Übersättigung und Überkaltung, *Zeitschrift Für Physikalische Chemie.* 22U (1897) 289–330. <https://doi.org/doi:10.1515/zpch-1897-2233>.
- [51] H. Zhang, J. F. Banfield, Thermodynamic analysis of phase stability of nanocrystalline titania, *J. Mater. Chem.* 8 (1998) 2073–2076. <https://doi.org/10.1039/A802619J>.
- [52] R.D. Shannon, Revised effective ionic radii and systematic studies of interatomic distances in halides and chalcogenides, *Acta Crystallographica Section A.* 32 (1976) 751–767. <https://doi.org/10.1107/S0567739476001551>.

- [53]D.L. Evans, Solid Solution of TiO₂ in SiO₂, *Journal of the American Ceramic Society*. 53 (1970) 418–418. <https://doi.org/10.1111/j.1151-2916.1970.tb12146.x>.
- [54]O.S. Dymshits, A.A. Zhilin, V.I. Petrov, M.Ya. Tsenter, T.I. Chuvaeva, V.V. Golubkov, A Raman spectroscopic study of phase transformations in titanium-containing lithium aluminosilicate glasses, *Glass Physics and Chemistry*. 24 (1998) 79–96.
- [55]B.O. Mysen, F.J. Ryerson, D. Virgo, The influence of TiO₂ on the structure and derivative properties of silicate melts, *American Mineralogist*. 65 (1980) 1150–1165.